Reliable source of conditional states from single-mode pulsed thermal fields by multiple-photon subtraction

A. Allevi,[1,*] A. Andreoni,[1,2] M. Bondani,[1,3] M. G. Genoni,[4,5] and S. Olivares[4,5,†]

[1]*Consorzio Nazionale Interuniversitario per le Scienze Fisiche della Materia U.d.R. Como, I-22100 Como, Italy*

[2]*Dipartimento di Fisica e Matematica, Università degli Studi dell'Insubria, I-22100 Como, Italy*

[3]*Istituto di Fotonica e Nanotecnologie, Consiglio Nazionale delle Ricerche, I-22100 Como, Italy*

[4]*Consorzio Nazionale Interuniversitario per le Scienze Fisiche della Materia U.d.R. Milano Università, I-20133 Milano, Italy*

[5]*Dipartimento di Fisica, Università degli Studi di Milano, I-20133 Milano, Italy*

(Received 30 March 2010; published 14 July 2010)

We demonstrate the effect of multiple-photon subtraction on the generation of conditional states in the pulsed regime. Our experimental scheme relies on a beam splitter (BS) and a pair of linear photodetectors that are able to resolve up to tens of photons. We use a single-mode thermal field at the input port of the BS to test the reliability of our scheme, and we show good agreement with the theory by fully characterizing the conditional outgoing states in terms of photon-number statistics and non-Gaussianity.

DOI: 10.1103/PhysRevA.82.013816 PACS number(s): 42.50.Dv, 03.67.−a, 85.60.Gz

I. INTRODUCTION

The subtraction of photons from an optical field is of both fundamental and practical interest, as it is linked to the properties of the annihilation operator [1] and plays a leading role in quantum information protocols involving non-Gaussian state generation, manipulation, and distillation [2–4]. In fact, the simplest way to generate a non-Gaussian optical state by starting from a Gaussian one consists of subtracting photons from it [5]. Photon subtraction can be implemented by inserting a beam splitter (BS) in the optical path of the original state, by detecting the number of photons at one output port, and by selecting the output of the other port only if a certain condition on the number of detected photons is satisfied. As we use short-pulsed fields, the challenging part of this scheme is the shot-by-shot measurement of sizable numbers of photons. As a matter of fact, it is nowadays quite easy to detect a single photon (see, e.g., Ref. [6] and references therein), while the limited availability of genuine photon counters has led to the quest for indirect ways to measure photon numbers in light pulses [7–9].

It is worth mentioning that the subtraction of photons allows not only the generation of non-Gaussian states, but also the enhancement of the nonlocality of bipartite states [10–14], or the generation of highly nonclassical states [15–17] useful for quantum information purposes [18]. Moreover, non-Gaussianity is a necessary ingredient for continuous-variable entanglement distillation [19–21] and different protocols, which rely on Gaussification of entangled non-Gaussian states [22–24] or on de-Gaussification of entangled Gaussian states, have been proposed [4]. In all these approaches, an important role is played by photodetectors able to perform reliable conditional measurements.

In this paper, we report a thorough analysis of a setup based on hybrid photodetectors, which allow the discrimination of up to tens of the number of detected photons [25,26]. The aim of the paper is twofold: First, we demonstrate the feasibility of our setup and, second, we investigate its reliability by characterizing the generated conditional states. The input states we employ to achieve these goals are single-mode thermal fields. Although photon-subtracted thermal states are not directly involved in any quantum information protocol, they are suitable probes to investigate the performances of our particular scheme. In fact, thermal states are Gaussian states diagonal in the photon-number basis, thus, the knowledge of their photon statistics fully characterizes them and their conditional non-Gaussian counterparts, which are still diagonal. Thanks to this property, we can give a complete analytical description of the behavior of our setup, which includes the actual expressions of the conditional states, and we can verify, with very high accuracy and control, the agreement of the theoretical expectations with the experimental results. This is a fundamental test in view of the application of our setup to more sophisticated cases, which involve nonclassical, multipartite, and multimode fields [27], including states whose conditional counterparts cannot be fully characterized analytically, in which case, the certified reliability of our scheme becomes crucial.

Throughout the paper, we investigate two possible scenarios. We refer to the first one as conclusive photon subtraction (CPS): A photon-number-resolving detector is used to condition the signal and to *conclude* which is the effective number of subtracted photons. The second one is the inconclusive photon subtraction (IPS): an on-off Geiger-like detector (i.e., a detector only able to distinguish the presence from the absence of photons is employed), which prevents us from inferring the actual number of subtracted photons. The paper is structured as follows. Section II addresses the generation of conditional states by means of detectors with an effective photon-number-resolving power. We discuss the model in the presence of nonunit quantum efficiency and give some analytical results. In Sec. III, we briefly review the IPS process on thermal Gaussian fields; we also investigate the main properties of the generated conditional non-Gaussian states that will turn out to be useful for the characterization of our setup. In Sec. IV, we report the experimental demonstration of our scheme and thoroughly characterize the obtained conditional states. Section V closes the paper and draws some concluding remarks.

*alessia.allevi@uninsubria.it

†stefano.olivares@mi.infn.it

II. CONDITIONAL NON-GAUSSIAN STATES FROM THERMAL FIELDS VIA CONDITIONAL MEASUREMENTS

In Fig. 1, we depict the conditional photon-subtraction scheme based on a BS and two photon-number-resolving detectors. Although, in our experimental realization, we will consider only thermal states, for the sake of generality, here, we consider a diagonal state of the form $\varrho = \sum_n \varrho_n |n\rangle\langle n|$. After the evolution through the BS with transmissivity τ, the initial two-mode state $R_0 = \varrho \otimes |0\rangle\langle 0|$ is transformed into the state,

$$R = \sum_{n=0}^{\infty} \varrho_n \sum_{k,l=0}^{n} A_k^n(\tau) A_l^n(\tau) |n-k\rangle\langle n-l| \otimes |k\rangle\langle l|, \tag{1}$$

where $A_s^n(\tau) = \sqrt{\binom{n}{s} \tau^{n-s}(1-\tau)^s}$. Then, the reflected part of the beam undergoes measurement. The positive-operator-valued measure (POVM), which describes a realistic photon-counting device with quantum efficiency η, is given by [28]

$$\Pi_m(\eta) = \sum_{s=m}^{\infty} B_{s,m}(\eta) |s\rangle\langle s|, \tag{2}$$

in which $B_{s,m}(\eta) = \binom{s}{m} \eta^m (1-\eta)^{s-m}$. If the photon counter in the reflected beam detects m_{R} photons, the CPS state obtained in the transmitted beam is

$$\begin{aligned} \varrho_{\mathrm{CPS}}(m_{\mathrm{R}}) &= \frac{1}{p_{\mathrm{R}}(m_{\mathrm{R}})} \mathrm{Tr}_{\mathrm{R}} \left[R\, \mathbb{I} \otimes \Pi_{m_{\mathrm{R}}}(\eta_{\mathrm{R}}) \right] \\ &= \frac{1}{p_{\mathrm{R}}(m_{\mathrm{R}})} \sum_{s=m_{\mathrm{R}}}^{\infty} \sum_{n=0}^{\infty} B_{s,m_{\mathrm{R}}}(\eta_{\mathrm{R}}) \\ &\quad \times \varrho_{s+n} \left[A_s^{s+n}(\tau) \right]^2 |n\rangle\langle n|, \end{aligned} \tag{3}$$

where η_k is the quantum efficiency of the detector located in the reflected ($k = \mathrm{R}$) and in the transmitted ($k = \mathrm{T}$) beam paths, respectively. Note that the state in Eq. (3) is still diagonal. The overall probability $p_{\mathrm{R}}(m_{\mathrm{R}})$ of measuring m_{R} in the reflected beam reads

$$p_{\mathrm{R}}(m_{\mathrm{R}}) = \sum_{s=m_{\mathrm{R}}}^{\infty} \sum_{n=0}^{\infty} B_{s,m_{\mathrm{R}}}(\eta_{\mathrm{R}}) \varrho_{n+s} \left[A_s^{n+s}(\tau) \right]^2, \tag{4}$$

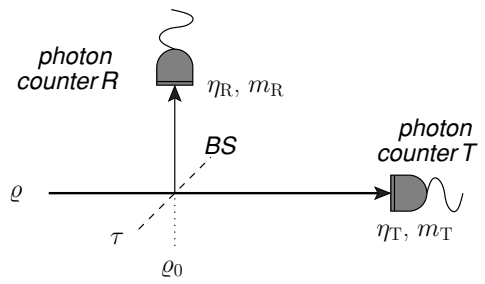

FIG. 1. Scheme for the generation of conditional non-Gaussian states via photon subtraction. A thermal input state ϱ is mixed with the vacuum state $\varrho_0 = |0\rangle\langle 0|$ at a BS with transmissivity τ. Two photon counters (R, T) with quantum efficiency η_k, $k = \mathrm{R,T}$ are used to generate and to analyze conditional states. See text for details.

which represents the marginal distribution of the joint probability,

$$\begin{aligned} p_{\mathrm{TR}}(m_{\mathrm{T}}, m_{\mathrm{R}}) &= \mathrm{Tr} \left[R\, \Pi_{m_{\mathrm{T}}}(\eta_{\mathrm{T}}) \otimes \Pi_{m_{\mathrm{R}}}(\eta_{\mathrm{R}}) \right] \\ &= \sum_{t=m_{\mathrm{T}}}^{\infty} \sum_{s=m_{\mathrm{R}}}^{\infty} B_{s,m_{\mathrm{R}}}(\eta_{\mathrm{R}})\, B_{t,m_{\mathrm{T}}}(\eta_{\mathrm{T}}) \left[A_s^{s+t}(\tau) \right]^2 \varrho_{s+t}, \end{aligned} \tag{5}$$

that detectors T and R measure m_{T} and m_{R} photons, respectively. By taking ϱ in a single-mode thermal state $\nu(N_{\mathrm{th}})$,

$$\nu(N_{\mathrm{th}}) = \sum_{n=0}^{\infty} \nu_n(N_{\mathrm{th}}) |n\rangle\langle n|, \tag{6}$$

$$\nu_n(N_{\mathrm{th}}) = \frac{1}{1+N_{\mathrm{th}}} \left(\frac{N_{\mathrm{th}}}{1+N_{\mathrm{th}}} \right)^n, \tag{7}$$

where N_{th} denotes the mean number of thermal photons, Eq. (5) reduces to

$$p_{\mathrm{TR}}(m_{\mathrm{T}}, m_{\mathrm{R}}) = \binom{m_{\mathrm{T}} + m_{\mathrm{R}}}{m_{\mathrm{R}}} \frac{M_{\mathrm{T}}{}^{m_{\mathrm{T}}}\, M_{\mathrm{R}}{}^{m_{\mathrm{R}}}}{(1 + M_{\mathrm{T}} + M_{\mathrm{R}})^{m_{\mathrm{T}}+m_{\mathrm{R}}+1}}, \tag{8}$$

where $M_{\mathrm{T}} = \tau\, \eta_{\mathrm{T}}\, N_{\mathrm{th}}$ and $M_{\mathrm{R}} = (1-\tau)\, \eta_{\mathrm{R}}\, N_{\mathrm{th}}$ are the mean numbers of detected photons of the transmitted and reflected beams, respectively.

Given m_{R} and $p_{\mathrm{R}}(m_{\mathrm{R}})$, the conditional state ϱ_{CPS} in Eq. (3) can be obtained straightforwardly. From Eq. (3), we can then evaluate the Fano factor,

$$F_{\mathrm{CPS}} = \frac{\sigma^2(M_{\mathrm{CPS}})}{M_{\mathrm{CPS}}}, \tag{9}$$

which is the ratio between the variance $\sigma^2(M_{\mathrm{CPS}})$ and the mean number M_{CPS} of the photons detected in the CPS state. As we will see in what follows, $F_{\mathrm{T}} \geqslant F_{\mathrm{CPS}} \geqslant 1$, where $F_{\mathrm{T}} = 1 + M_{\mathrm{T}}$ is the Fano factor of the single-mode thermal field of the (unconditional) transmitted beam. Note that ϱ_{CPS} is always super-Poissonian, which is consistent with the classical nature of the field.

To deeply characterize the output conditional state, we evaluate its non-Gaussianity. Since the state has the form $\varrho_{\mathrm{CPS}} = \sum_n p_n |n\rangle\langle n|$, the non-Gaussianity measure [29] can be written as

$$\delta[\varrho_{\mathrm{CPS}}] = S[\nu(N_{\mathrm{CPS}})] + \sum_n p_n \log\, p_n, \tag{10}$$

where N_{CPS} is the mean photon number of ϱ_{CPS}, and $S[\nu(N)] = N \log(1 + 1/N) + \log(1+N)$ is the entropy of the thermal state $\nu(N)$.

However, due to the inefficient detection, we cannot reconstruct the actual photon-number distribution p_n, but only the *detected* photon-number distribution $q_{m_{\mathrm{T}}} = p_{\mathrm{TR}}(m_{\mathrm{T}}, m_{\mathrm{R}})$ given in Eq. (8), where m_{R} is the conditioning value, and m_{T} is the number of detected photons. Thus, we can evaluate the quantity:

$$\varepsilon[\varrho_{\mathrm{CPS}}] = S[\nu(M_{\mathrm{CPS}})] + \sum_{m_{\mathrm{T}}} q_{m_{\mathrm{T}}} \log\, q_{m_{\mathrm{T}}} \leqslant \delta[\varrho_{\mathrm{CPS}}]. \tag{11}$$

The last inequality follows from the fact that the inefficient detection may be described by a Gaussian lossy channel that does not increase the non-Gaussianity, followed by an ideal (i.e., unit quantum efficiency) detection (see the Appendix for

details). The quantity $\varepsilon[\varrho_{\rm CPS}]$, which can easily be evaluated from our experimental data, turns out to be a lower bound for the actual non-Gaussianity, that is, significant values of $\varepsilon[\varrho_{\rm CPS}]$ correspond to more markedly non-Gaussian states $\varrho_{\rm CPS}$.

III. INCONCLUSIVE PHOTON SUBTRACTION ON THERMAL STATES

The conditional states introduced in Sec. II can be generated only if the detector in the reflected beam path is able to resolve the number of incoming photons. In this section, we consider a scenario in which the detector R (see Fig. 1) can only distinguish the presence from the absence of light (Geiger-like detector): We will refer to this measurement as inconclusive, as it does not resolve the number of the detected photons. When the detector clicks, an unknown number of photons is subtracted from ϱ, and we obtain the IPS state $\varrho_{\rm IPS}$. To characterize this class of conditional state, we use the phase-space description of the system evolution, which allows a simpler analysis with respect to that based on the photon-number basis.

The phase-space description of the IPS operated on single-mode Gaussian states can be obtained by generalizing the analysis given in Ref. [16]. The Wigner function of the thermal state in Eq. (6) reads as follows (in Cartesian notation):

$$W_{\rm th}(\boldsymbol{X}) = \frac{\exp\left(-\frac{1}{2}\boldsymbol{X}^T\boldsymbol{\sigma}_{\rm th}^{-1}\boldsymbol{X}\right)}{2\pi\sqrt{\mathrm{Det}\,[\boldsymbol{\sigma}_{\rm th}]}}, \tag{12}$$

where

$$\boldsymbol{\sigma}_{\rm th} \equiv \boldsymbol{\sigma}_{\rm th}(N_{\rm th}) = \frac{1+2N_{\rm th}}{2}\,\mathbb{1} \tag{13}$$

is the covariance matrix (CM), with $\mathbb{1}$ as the 2×2 identity matrix. According to Ref. [16], the action of the BS transforms the CM of the two-mode input state (thermal + vacuum),

$$\boldsymbol{\sigma}_{\rm in} = \begin{pmatrix} \boldsymbol{\sigma}_{\rm th} & \boldsymbol{0} \\ \boldsymbol{0} & \boldsymbol{\sigma}_0 \end{pmatrix}, \tag{14}$$

as follows [30]:

$$\boldsymbol{\sigma}' \equiv \boldsymbol{S}_{\rm BS}^T(\tau)\,\boldsymbol{\sigma}_{\rm in}\,\boldsymbol{S}_{\rm BS}(\tau) \equiv \begin{pmatrix} \boldsymbol{A} & \boldsymbol{C} \\ \boldsymbol{C}^T & \boldsymbol{B} \end{pmatrix}, \tag{15}$$

where $\boldsymbol{A}$, $\boldsymbol{B}$, and $\boldsymbol{C}$ are 2×2 matrices, and

$$\boldsymbol{S}_{\rm BS}(\tau) = \begin{pmatrix} \sqrt{\tau}\mathbb{1} & \sqrt{1-\tau}\mathbb{1} \\ -\sqrt{1-\tau}\mathbb{1} & \sqrt{\tau}\mathbb{1} \end{pmatrix} \tag{16}$$

is the symplectic transformation associated with the evolution operator $U_{\rm BS}$ of the BS.

The probability $p_{\rm on} = p_{\rm on}(r,\tau,\eta_{\rm R})$ that the on-off detector endowed with quantum efficiency $\eta_{\rm R}$ clicks is given by [30]

$$p_{\rm on} = 1 - p_{\rm off}(r,\tau,\eta_{\rm R}) \tag{17}$$

$$= 1 - [\eta_{\rm R}\sqrt{\mathrm{Det}\,(\boldsymbol{B}+\boldsymbol{\sigma}_{\rm M})}]^{-1} \tag{18}$$

$$= \frac{\eta_{\rm R}(1-\tau)N_{\rm th}}{1+\eta_{\rm R}(1-\tau)N_{\rm th}}, \tag{19}$$

where $p_{\rm off}$ is the probability of a nonclick event, and

$$\boldsymbol{\sigma}_{\rm M} = \frac{2-\eta_{\rm R}}{2\eta_{\rm R}}\mathbb{1}. \tag{20}$$

The Wigner function associated with the IPS state $\varrho_{\rm IPS}$ reads

$$W_{\rm IPS}(\boldsymbol{X}) = \frac{W_a(\boldsymbol{X}) - p_{\rm off}\,W_b(\boldsymbol{X})}{p_{\rm on}}, \tag{21}$$

where

$$W_k(\boldsymbol{X}) = \frac{\exp\left(-\frac{1}{2}\boldsymbol{X}^T\boldsymbol{\Sigma}_k^{-1}\boldsymbol{X}\right)}{2\pi\sqrt{\mathrm{Det}\,[\boldsymbol{\Sigma}_k]}} \quad (k=a,b), \tag{22}$$

$\boldsymbol{\Sigma}_a = \boldsymbol{A}$ and $\boldsymbol{\Sigma}_b = \boldsymbol{A} - \boldsymbol{C}(\boldsymbol{B}-\boldsymbol{\sigma}_{\rm M})\boldsymbol{C}^T$. Note that the IPS, because it is the linear combination of two Gaussian functions, is no longer Gaussian: For this reason, the IPS process is also referred to as a *de-Gaussification* process [15]. The Wigner functions in Eq. (22) are those of two thermal states $\nu(N_k)$ with the mean number of photons N_k given by

$$N_a = \tau N_{\rm th}, \quad N_b = \frac{\tau N_{\rm th}}{1+\eta_{\rm R}(1-\tau)N_{\rm th}}, \tag{23}$$

respectively; thus, the density matrix associated with Eq. (21) can be written as

$$\varrho_{\rm IPS} = \frac{\nu(N_a) - p_{\rm off}\,\nu(N_b)}{p_{\rm on}}, \tag{24}$$

and the corresponding conditional distribution of the detected photons is

$$p_T(m_{\rm T}) = \frac{\nu_{m_{\rm T}}(M_a) - p_{\rm off}\,\nu_{m_{\rm T}}(M_b)}{p_{\rm on}}, \tag{25}$$

where $M_a = \eta_{\rm T}N_a$ and $M_b = \eta_{\rm T}N_b$, $\eta_{\rm T}$ is the quantum efficiency of the photon-resolving detector of the IPS state, and $\nu(N_k)$ are given by Eq. (7).

By starting from the previous results, we can give further details about the IPS thermal state in Eq. (24). The mean number of detected photons is

$$M_{\rm IPS} = \frac{M_a - p_{\rm off}\,M_b}{p_{\rm on}}, \tag{26}$$

and the variance $\sigma^2(M_{\rm IPS})$ is

$$\sigma^2(M_{\rm IPS}) = \frac{M_a(1+M_a) - p_{\rm off}\,M_b(1+M_b)}{p_{\rm on}} - \frac{p_{\rm off}(M_a-M_b)^2}{p_{\rm on}^2}. \tag{27}$$

Moreover, as $M_a \geqslant M_b$, the Fano factor $F_{\rm IPS}$ is

$$F_{\rm IPS} = \frac{\sigma^2(M_{\rm IPS})}{M_{\rm IPS}} \tag{28}$$

$$= 1 + M_b + 2\frac{M_a(M_a-M_b)}{M_a - p_{\rm off}\,M_b} - \frac{M_a-M_b}{1-p_{\rm off}} \geqslant 1, \tag{29}$$

in which the final inequality can be checked by substituting the actual expressions of M_a, M_b, and $p_{\rm off}$. The state is always super-Poissonian (also, in this case, as one would expect, $F_{\rm T} \geqslant F_{\rm IPS} \geqslant 1$). As for the conditional states $\varrho_{\rm CPS}$, we can characterize the non-Gaussianity of the state $\varrho_{\rm IPS}$ from the experimental data by evaluating the quantity,

$$\varepsilon[\varrho_{\rm IPS}] = S[\nu(M_{\rm IPS})] + \sum_{m_{\rm T}} q_{m_{\rm T}} \log\, q_{m_{\rm T}}\,, \tag{30}$$

which is still a lower bound for the non-Gaussianity measure (i.e. $\varepsilon[\varrho_{\mathrm{IPS}}] \leqslant \delta[\varrho_{\mathrm{IPS}}]$) as explained in more detail in Sec. II and in the Appendix.

IV. RELIABLE SOURCE OF NON-GAUSSIAN STATES

A. Experimental setup

We produced a single-mode pseudothermal state by inserting a rotating ground-glass plate in the pathway of a coherent field, followed by a pin hole to select a single coherence area in the far-field speckle pattern (see Fig. 2). As most detectors have the maximum quantum efficiency in the visible spectral range, we chose to exploit the second-harmonic linearly polarized pulses ($\lambda = 523$ nm, 5.4-ps pulse duration) of an Nd:yttrium-lithium-fluoride mode-locked laser amplified at 500 Hz. The thermal light was split into two parts by a polarizing cube beam splitter (PBS) whose transmissivity τ can be continuously varied by means of a half-wave plate ($\lambda/2$ in Fig. 2). We balanced the two exiting arms of the PBS to achieve $\tau \simeq 0.5$. The light exiting the PBS was focused in two multimode fibers and was delivered to two hybrid photodetectors ([$\mathrm{HPD_{R,T}}$], model R10467U-40, Hamamatsu), endowed not only with a partial photon-resolving capability, but also with a linear response up to 100 incident photons. The outputs of the detectors were amplified (preamplifier A250 plus amplifier A275, Amptek), synchronously integrated (SGI, SR250, Stanford), digitized (ATMIO-16E-1, National Instruments), and processed off-line. To analyze the outputs, we model the detection process as a Bernoullian convolution and the overall amplification-conversion process through a very precise constant factor γ, which allows the shot-by-shot detector output to be converted into a number of detected photons [31,32]. The calibration procedure required performing a set of measurements of the light at different values of the overall detection efficiency of the apparatus η set by rotating a continuously variable neutral-density filter wheel placed in front of the $\lambda/2$ plate. For each value of η, we recorded the data from 30 000 subsequent laser shots. For the results presented in the following, we obtained the values $\gamma_{\mathrm{R}} = 0.104$ V and $\gamma_{\mathrm{T}} = 0.093$ V for the calibration of the detection chains in the reflected and transmitted arms of the BS, respectively. These values of $\gamma_{\mathrm{R,T}}$ were used to convert the voltages into the number of detected photons that were finally rebinned into unitary bins to obtain probability distributions. Once checked the reliability of the calibrations from the quality of these distributions, the voltage outputs of the $\mathrm{HPD_{R,T}}$ detectors were associated with numbers m_{R} and m_{T} in real time. The linearity of the detectors and the absence of significant dark counts make our system suitable for conducting experiments in both the CPS and the IPS scenarios to produce conditional states. In the case of IPS, we only distinguish the $\mathrm{HPD_R}$ outputs that give $m_{\mathrm{R}} = 0$ from those that give any $m_{\mathrm{R}} \geqslant 1$ to mimic the behavior of a Geiger-like detector.

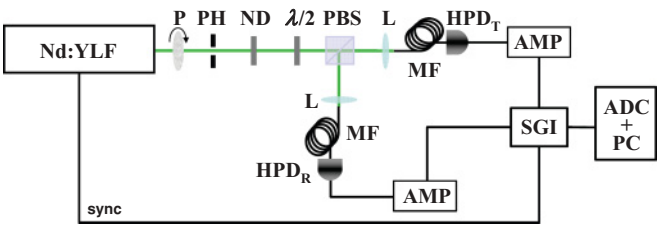

FIG. 2. (Color online) Scheme of the experimental setup: P, rotating ground-glass plate; PH, pin hole; ND, continuously variable neutral-density filter; $\lambda/2$, half-wave plate; PBS, polarizing cube beam splitter; L, collective lens; MF, multimode fiber; $\mathrm{HPD_{R,T}}$, hybrid photodetector; AMP, preamplifier plus amplifier; SGI, synchronous-gated integrator; ADC + PC, analog-to-digital converter.

B. Conditional non-Gaussian states

The good photon-resolving capability of HPD detectors and their linearity make it possible to implement the CPS scheme described in Sec. II. Conditional measurements in the reflected beam irreversibly modify the states measured in the transmitted arm and, in particular, make them non-Gaussian.

To better understand the power and the limits of this kind of conditioning operation, we follow two different approaches: First of all, we fix the energy N_{th} of the initial thermal field and characterize the CPS state as a function of the conditioning value m_{R}. Second, we consider the properties of CPS states as a function of the mean incoming photons N_{th} for a particular choice of the number m_{R} of photons detected in the reflected arm. The final aim is the production of non-Gaussian states with a well-defined conditioning value.

We start by presenting the results obtained by choosing a set of measurements with $M_{\mathrm{T}} \approx 1.254$.

The joint probability $p_{\mathrm{TR}}(m_{\mathrm{T}},m_{\mathrm{R}})$ of measuring m_{R} photons in the reflected arm and m_{T} photons in the transmitted one is plotted in Fig. 3 as dots together with the theoretical surface to which they perfectly superimpose. Of course, by starting from the theoretical joint probability, we can calculate the expected photon-number distribution of the states obtained by performing different conditional measurements in the reflected arm [see Eq. (3)] and, thus, evaluate all the quantities necessary to characterize the CPS states.

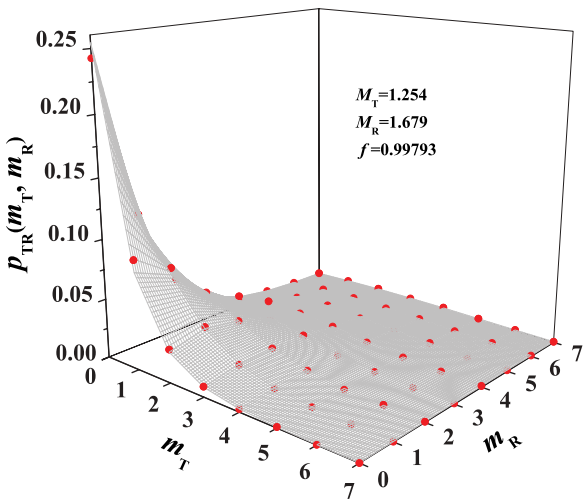

FIG. 3. (Color online) Joint probability $p_{\mathrm{TR}}(m_{\mathrm{T}},m_{\mathrm{R}})$ to measure m_{R} photons in the reflected beam and m_{T} photons in the transmitted one. The experimental data (red dots) are plotted together with the theoretical surface (gray mesh). The other involved experimental values are $M_{\mathrm{R}} = 1.679$ and $M_{\mathrm{T}} = 1.254$.

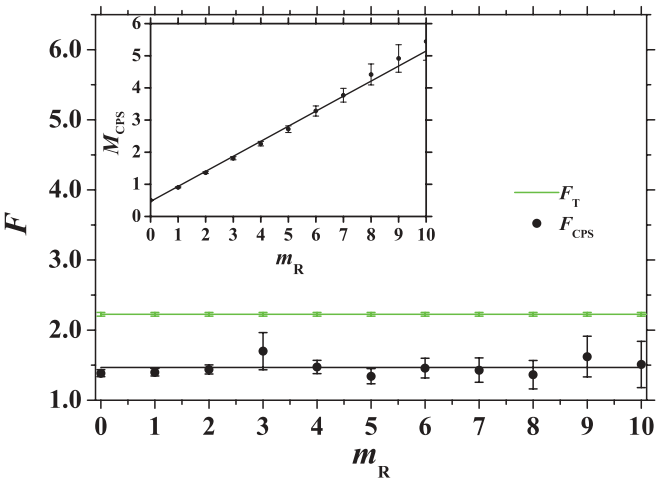

FIG. 4. (Color online) Fano factors $F_{\rm CPS}$ of the conditional states: experiment (black dots) and theory [solid black (lower) line] as functions of the conditioning value $m_{\rm R}$. The green (higher) line corresponds to the Fano factor $F_{\rm T} = 1 + M_{\rm T}$ of the (unconditional) transmitted state. The inset refers to mean number of detected photons $M_{\rm CPS}$ of the CPS states as a function of the conditioning value $m_{\rm R}$: experimental data (dots) and theoretical curve (solid line). The values of the other involved parameters are $M_{\rm R} = 1.679$ and $M_{\rm T} = 1.254$.

In Fig. 4, we plot the behavior of the mean number of photons $M_{\rm CPS}$ of the conditional states and their Fano factors $F_{\rm CPS}$ as a function of the different conditioning values $m_{\rm R}$. We find that the Fano factor does not depend on the particular choice of the conditioning value $m_{\rm R}$, in agreement with the analytical result calculated from Eq. (8):

$$F_{\rm CPS} = \frac{1 + M_{\rm T} + M_{\rm R}}{1 + M_{\rm R}} \approx 1.468. \tag{31}$$

Note that the obtained value is definitely lower than that of the unconditional state $F_{\rm T} \approx 2.225$.

The photon-number distributions of the conditional states look quite different from each other. As shown in Fig. 5, the larger the conditioning value, the more different the statistics of the conditional state (colored symbols + lines) is from that of the incoming one (black triangles + dashed line). We note that, due to the limited number of recorded shots (only 30 000 laser shots), the experimental points tend to deviate from the expected $p_{\rm T}$ distributions at increasing conditioning values. This behavior can be quantified by calculating the fidelity (see f values reported in Fig. 5): $f = \sum_{m=0}^{\bar{m}} \sqrt{p_{\rm T}^{\rm th}(m)\, p_{\rm T}(m)}$, in which $p_{\rm T}^{\rm th}(m)$ and $p_{\rm T}(m)$ are the theoretical and experimental distributions, respectively, and the sum is extended up to the maximum detected photon number $\bar{m}$ above which both $p_{\rm T}^{\rm th}(m)$ and $p_{\rm T}(m)$ become negligible. For all data displayed in Fig. 5, the fidelity is rather satisfactory.

Finally, the behavior of the lower bound for the non-Gaussianity measure as a function of the conditioning value $m_{\rm R}$ (Fig. 6) predicted by the theory (line) is well reproduced by the experimental data (dots). In particular, it is worth noting that the value of $\varepsilon[\varrho_{\rm CPS}]$ increases at increasing the conditioning value.

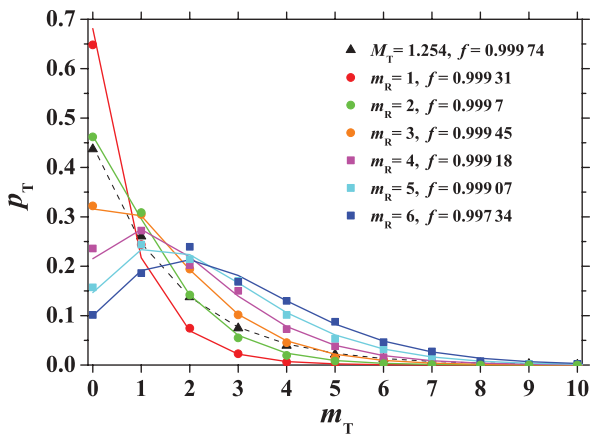

FIG. 5. (Color online) Reconstructed photon-number distributions of the (unconditional) thermal state with mean number of photons $M_{\rm T} = 1.254$ (black triangles) and of the conditional states for six different conditioning values $m_{\rm R}$ (colored dots and squares). The theoretical curves are plotted as lines according to the same choice of colors. The corresponding fidelity f is also reported.

As an example of the second approach, we consider the CPS states obtained by choosing $m_{\rm R} = 2$ as the conditioning value for different values of $N_{\rm th}$. In the inset of Fig. 7, the mean number of photons of the CPS states is plotted together with the mean number of photons of the initial states measured in the transmitted arm: It is interesting to notice that the values of $M_{\rm CPS}$ actually approach the conditioning value $m_{\rm R} = 2$. Again, the experimental results (dots) are well superimposed to the theoretical curves, calculated starting from Eq. (3) with the measured mean values.

Figure 7 also shows the comparison between the Fano factor of the unconditional states $F_{\rm T}$ (green squares) and that of the CPS states $F_{\rm CPS}$ (black dots): As expected from the theory, the conditional states preserve the super-Poissonian nature of the incoming states, although with a smaller value of the Fano factor ($F_{\rm T} \geqslant F_{\rm CPS} \geqslant 1$).

In Fig. 8, we show three examples of conditional-state photon distributions for different values of the total incident

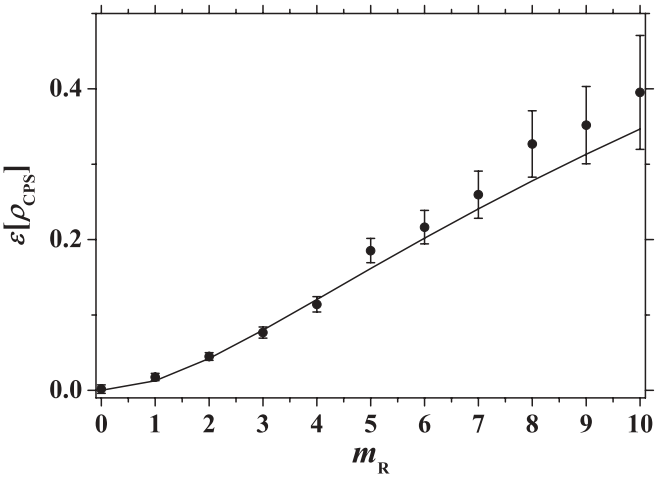

FIG. 6. Lower bound $\varepsilon[\varrho_{\rm CPS}]$ for the non-Gaussianity measure $\delta[\varrho_{\rm CPS}]$ as a function of the conditioning value $m_{\rm R}$ for $M_{\rm T} = 1.254$.

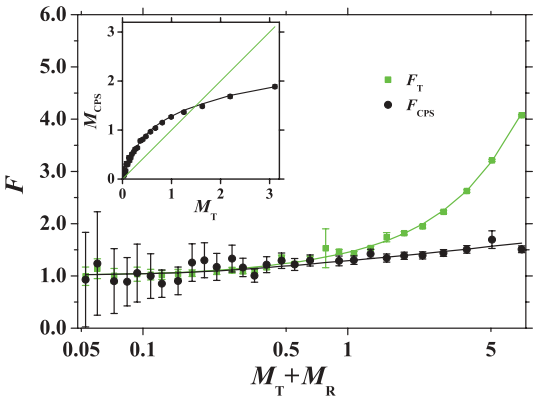

FIG. 7. (Color online) Log-linear plot of the Fano factors F_{CPS} of the CPS states (black dots) and of the unconditional states F_{T} (green squares) as functions of the total mean detected photons $M_{\mathrm{T}} + M_{\mathrm{R}}$ for conditioning $m_{\mathrm{R}} = 2$. The solid lines refer to the corresponding theoretical curves. The inset shows the mean number of detected photons M_{CPS} of the CPS states as a function of the mean number of detected photons M_{T} of the unconditional states: experimental data (black dots) and theoretical curve (solid line). The green (straight) line refers to the mean photon number M_{T} of the unconditional states.

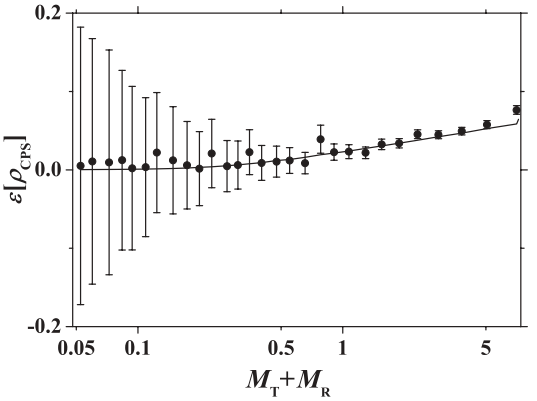

FIG. 9. Log-linear plot of the lower bound $\varepsilon[\varrho_{\mathrm{CPS}}]$ for the non-Gaussianity $\delta[\varrho_{\mathrm{IPS}}]$ as a function of the total mean detected photons $M_{\mathrm{T}} + M_{\mathrm{R}}$ and for $m_{\mathrm{R}} = 2$: experimental data (dots) and theoretical curve (solid line).

intensity. For each example, we plot both the original thermal distribution (full symbols) and that of the conditional state (empty symbols). The agreement with the corresponding theoretical predictions (lines) is again witnessed by the high value of the fidelities.

In Fig. 9, we plot the lower bound for the non-Gaussianity $\varepsilon[\varrho_{\mathrm{CPS}}]$ as a function of the total mean detected photons (see Fig. 9) together with the expected theoretical results.

C. IPS non-Gaussian states

Here, we consider the scenario in which an on-off Geiger-like detector measures the reflected part of the input signal. In particular, as described in Sec. III, we are interested in studying the properties of the state produced in the transmitted arm of the PBS whenever the detector placed in the reflected arm clicks. To this aim, we performed a set of measurements by fixing the transmissivity of the PBS $\tau = 0.5$ and by changing the mean intensity of the light that impinges on the PBS.

In the inset of Fig. 10, we plot the mean number of detected photons M_{IPS} of the IPS states as a function of the mean number of detected photons M_{T} of the unconditional thermal states (black dots) together with the theoretical prediction (solid line) according to Eq. (26). We note that the effect of the conditioning operation is to increase the mean value of the original state. As described in Sec. III, another quantity to characterize the IPS state is the Fano factor F_{IPS}: To better appreciate the difference between the unconditional states and the corresponding conditional ones, in Fig. 10 we plot the corresponding Fano factors as functions of the total mean detected photons (symbols). For each set of experimental results, we

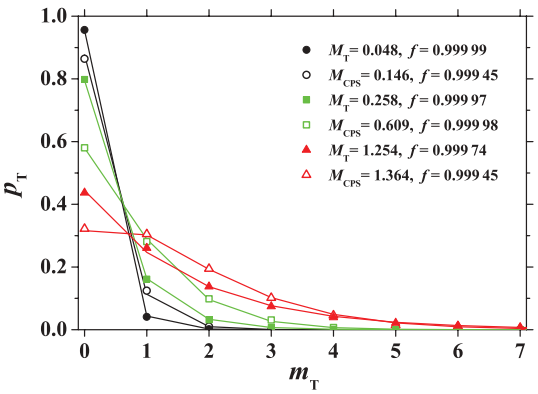

FIG. 8. (Color online) Reconstructed photon-number distributions for three different examples [black (lowest), green (middle), red (highest)] of unconditional states (full symbols) and for the corresponding CPS states (empty symbols) with $m_{\mathrm{R}} = 2$. The theoretical curves are plotted as lines according to the same choice of colors. The corresponding fidelity f is also reported.

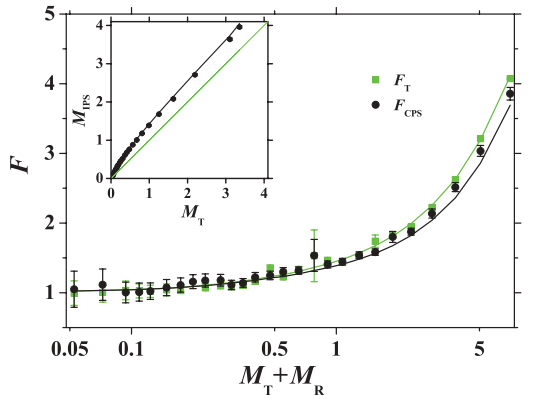

FIG. 10. (Color online) Log-linear plot of the Fano factors F_{IPS} of the IPS states (black dots) and of the unconditional states (green squares) as functions of the total mean detected photons $M_{\mathrm{T}} + M_{\mathrm{R}}$. The solid lines refer to the corresponding theoretical curves. The inset shows the mean number of detected photons M_{IPS} of the IPS states as a function of the mean number of detected photons M_{T} of the unconditional states: experimental data (black dots) and theoretical curve [solid (higher) line]. The green (lower) line refers to the mean photon number M_{T} of the unconditional states.

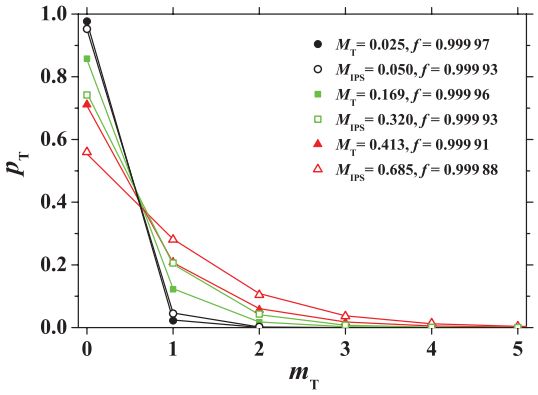

FIG. 11. (Color online) Reconstructed photon-number distributions for three different examples [black (lowest), green (middle), red (highest)] of unconditional states (full symbols) and for the corresponding IPS states (empty symbols). The theoretical curves are plotted as lines according to the same choice of colors. The fidelity f is also reported.

also plot the theoretical behaviors (lines): Analogous to the conditional case, we have $F_T \geqslant F_{IPS} \geqslant 1$.

In Fig. 11, we show the reconstruction of the *detected* photons distribution $p_T(m_T)$ of both the unconditional (full symbols) and the conditional states (empty symbols) for three different mean values [black (lowest), green (middle), red (highest)] of the incident intensity. The agreement with the corresponding theoretical distributions [colored (middle and highest) lines], calculated with the measured mean values, can be checked by evaluating the fidelity, as reported in Fig. 11.

Finally, in Fig. 12, we plot the lower bound for the non-Gaussianity measure $\varepsilon[\varrho_{IPS}]$ as a function of the total mean detected photons. The correspondence between the experimental results (dots) and the theoretical prediction (line) is good. Note that $\varepsilon[\varrho_{IPS}]$ increases as the mean number of detected photons increases: This allows the generation of highly populated non-Gaussian states.

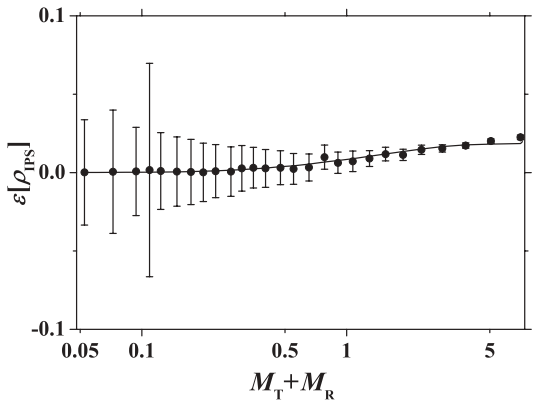

FIG. 12. Log-linear plot of the lower bound $\varepsilon[\varrho_{IPS}]$ for the non-Gaussianity $\delta[\varrho_{IPS}]$ as a function of the total mean detected photons $M_T + M_R$: experimental data (dots) and theoretical curve (line).

V. CONCLUDING REMARKS

In this paper, we have discussed in detail, both from a theoretical and an experimental point of view, a setup based on a single BS and two photon-number-resolving detectors to subtract photons from an incoming state and, thus, to generate non-Gaussian states by starting from Gaussian ones. In order to show the reliability of our setup, we used (Gaussian) thermal states as input probes and completely characterized the conditional photon-subtracted non-Gaussian outgoing states. In our analysis, we adopted two possible detection schemes: The first one is based on the CPS; whereas the second one is based on the IPS. In particular, we have demonstrated, as one may expect, that the non-Gaussianity of a state increases by increasing either the intensity of the input states or the conditioning value in the CPS scenario. This last condition requires photon-counting detectors endowed with a good linear response, such as those used in our experiment.

The use of thermal states, a class of states diagonal in the photon-number basis, allows us to obtain high-degree controls in both analytical theoretical expectations and experimental realization, which is a key point in possible further investigations. In particular, we are planning to apply our scheme to more exotic classical states, such as the phase-averaged coherent states [25]. As these are already non-Gaussian, the possibility to perform conditional non-Gaussian measurements on them would be particularly intriguing. Since analytical calculations may be carried out only to a certain extent in this case, we would provide an example in which the reliability of the setup is fundamental, as theoretical expectations are limited to numerical results.

Although we only focused on classical states, our experimental procedure could be applied to nonclassical states in order to obtain more sophisticated quantum fields [27,32], which may be useful for quantum information protocols involving photon-subtracted non-Gaussian states [3,10–12,17], such as entanglement distillation protocols [4,22,23].

ACKNOWLEDGMENTS

We thank M. G. A. Paris for his encouragement, advise, and careful critical reading of this manuscript, V. C. Usenko and S. Cialdi for useful discussions, and M. S. Kim and P. Marek for useful suggestions. This work has been partially supported by the CNR-CNISM agreement.

APPENDIX: EXPERIMENTAL LOWER BOUND FOR THE NON-GAUSSIANITY

For a single-mode state diagonal in the Fock basis (i.e., $\varrho = \sum_n p_n |n\rangle\langle n|$), the non-Gaussianity measure [29] is given by

$$\delta[\varrho] = S[\nu(N)] - S(\varrho) = S[\nu(N)] + \sum_n p_n \log p_n, \quad \text{(A1)}$$

where $\nu(N)$ is a thermal state with mean photon number $N = \sum_n n\, p_n$. As it is based on the knowledge of the actual photon distribution p_n, the calculation of $\delta[\varrho]$ requires measuring with an ideal (i.e., with unit quantum efficiency) photon-number resolving detector. In the presence of inefficient detection,

one can only retrieve the *detected* photon number distribution $q_m = \mathrm{Tr}\,[\varrho\Pi_m(\eta)]$, where $\Pi_m(\eta)$ is given in Eq. (2) and η is the quantum efficiency. Nevertheless, in the following, we will show that the quantity,

$$\varepsilon[\varrho] = S[\nu(M)] + \sum_m q_m \log q_m, \tag{A2}$$

where $M = \sum_m m$ and $q_m = \eta N$, is a lower bound for the real non-Gaussianity $\delta[\varrho]$ (i.e., $\varepsilon[\varrho] \leqslant \delta[\varrho]$). Note that since $\varepsilon[\varrho]$ depends only on q_m, it can be calculated by starting from the experimental results.

The inefficient photodetection process can be described by mixing the quantum state ϱ with the vacuum at a BS with transmissivity η followed by perfect detection on the transmitted beam, to obtain

$$q_m = \mathrm{Tr}[\mathcal{E}(\varrho)|m\rangle\langle m|], \tag{A3}$$

where $\mathcal{E}(\varrho) = \mathrm{Tr}_2[U_{\mathrm{BS}}(\eta)\varrho \otimes |0\rangle\langle 0| U_{\mathrm{BS}}^{\dagger}(\eta)]$ is the lossy Gaussian channel. Since ϱ is diagonal in the Fock basis, $\mathcal{E}(\varrho)$ is still diagonal,

$$\mathcal{E}(\varrho) = \sum_n p_n \mathcal{E}(|n\rangle\langle n|) = \sum_m q_m |m\rangle\langle m|, \tag{A4}$$

in which $q_m = \sum_{n=m}^{\infty} p_n B_{n,m}(\eta)$. To obtain $\mathcal{E}(\varrho)$, we used $\mathcal{E}(|n\rangle\langle n|) = \sum_{l=0}^{n} B_{n,l}(\eta)|l\rangle\langle l|$, with $B_{n,l}(\eta)$ defined in Eq. (2). By using Eq. (A1), we obtain

$$\delta[\mathcal{E}(\varrho)] = S[\nu(M)] + \textstyle\sum_n q_n \log q_n = \varepsilon[\varrho]. \tag{A5}$$

As the non-Gaussianity measure $\delta[\varrho]$ is nonincreasing under Gaussian maps [29], we finally get

$$\varepsilon[\varrho] = \delta[\mathcal{E}(\varrho)] \leqslant \delta[\varrho]. \tag{A6}$$

To summarize, given a quantum state ϱ, diagonal in the Fock basis, we can measure the probability distribution of the detected photons q_m, and we can evaluate Eq. (A2) as a lower bound for the actual non-Gaussianity $\delta[\varrho]$.

[1] V. Parigi, A. Zavatta, M. Kim, and M. Bellini, Science **317**, 1890 (2007).
[2] M. S. Kim, J. Phys. B **41**, 133001 (2008).
[3] P. Marek and R. Filip, Phys. Rev. A **81**, 022302 (2010).
[4] H. Takahashi, J. S. Neergaard-Nielsen, M. Takeuchi, M. Takeoka, K. Hayasaka, A. Furusawa, and M. Sasaki, Nat. Photonics **4**, 178 (2010).
[5] A. Ourjoumtsev, R. Tualle-Brouri, and P. Grangier, Phys. Rev. Lett. **96**, 213601 (2006).
[6] V. Parigi, A. Zavatta, and M. Bellini, J. Phys. B **42**, 114005 (2009).
[7] A. R. Rossi, S. Olivares, and M. G. A. Paris, Phys. Rev. A **70**, 055801 (2004).
[8] G. Zambra, A. Andreoni, M. Bondani, M. Gramegna, M. Genovese, G. Brida, A. Rossi, and M. G. A. Paris, Phys. Rev. Lett. **95**, 063602 (2005).
[9] G. Brida, M. Genovese, A. Meda, S. Olivares, M. G. A. Paris, and F. Piacentini, J. Mod. Opt. **56**, 196 (2009).
[10] T. Opatrný, G. Kurizki, and D.-G. Welsch, Phys. Rev. A **61**, 032302 (2000).
[11] P. T. Cochrane, T. C. Ralph, and G. J. Milburn, Phys. Rev. A **65**, 062306 (2002).
[12] S. Olivares, M. G. A. Paris, and R. Bonifacio, Phys. Rev. A **67**, 032314 (2003).
[13] C. Invernizzi, S. Olivares, M. G. A. Paris, and K. Banaszek, Phys. Rev. A **72**, 042105 (2005).
[14] S. Olivares and M. G. A. Paris, Laser Phys. **16**, 1533 (2006).
[15] J. Wenger, R-Tualle-Brouri, and P. Grangier, Phys. Rev. Lett. **92**, 153601 (2004).
[16] S. Olivares and M. G. A. Paris, J. Opt. B: Quantum Semiclassical Opt. **7**, S616 (2005).
[17] T. Gerrits, S. Glancy, T. S. Clement, B. Calkins, A. E. Lita, A. J. Miller, A. L. Migdall, S. W. Nam, R. P. Mirin, E. Knill, e-print arXiv:1004.2727v1 [quant-ph].
[18] N. J. Cerf, O. Krüger, P. Navez, R. F. Werner, and M. M. Wolf, Phys. Rev. Lett. **95**, 070501 (2005).
[19] J. Eisert, S. Scheel, and M. B. Plenio, Phys. Rev. Lett. **89**, 137903 (2002).
[20] J. Fiurášek, Phys. Rev. Lett. **89**, 137904 (2002).
[21] G. Giedke and J. I. Cirac, Phys. Rev. A **66**, 032316 (2002).
[22] D. E. Browne, J. Eisert, S. Scheel, and M. B. Plenio, Phys. Rev. A **67**, 062320 (2003).
[23] J. Eisert, D. E. Browne, S. Scheel, and M. B. Plenio, Ann. Phys. (NY) **311**, 431 (2004).
[24] B. Hage, A. Franzen, J. DiGuglielmo, P. Marek, J. Fiurášek, and R. Schnabel, New J. Phys. **9**, 227 (2007).
[25] M. Bondani, A. Allevi, and A. Andreoni, Adv. Sci. Lett. **2**, 463 (2009).
[26] M. Bondani, A. Allevi, and A. Andreoni, Opt. Lett. **34**, 1444 (2009).
[27] A. Allevi, A. Andreoni, F. A. Beduini, M. Bondani, M. G. Genoni, S. Olivares, and M. G. A. Paris (unpublished).
[28] The most general POVM that describes a photon-counting device also takes the presence of the dark counts into account; however, for the photodetectors that we used in the experimental demonstration, the number of the dark counts was negligible.
[29] M. G. Genoni, M. G. A. Paris, and K. Banaszek, Phys. Rev. A **78**, 060303(R) (2008).
[30] A. Ferraro, S. Olivares, and M. G. A. Paris, *Gaussian States in Quantum Information* (Bibliopolis, Napoli, 2005).
[31] M. Bondani, A. Allevi, A. Agliati, and A. Andreoni, J. Mod. Opt. **56**, 226 (2009).
[32] M. G. Genoni, F. A. Beduini, A. Allevi, M. Bondani, S. Olivares, and M. G. A. Paris, Physica Scripta (to be published).